Improved Cycling Performance of Intermetallic Anode by Minimized SEI Layer Formation

Kuwata, Hiroko ; Matsui, Masaki ; Sonoki, Hidetoshi ; Manabe, Yusuke ; Imanishi, Nobuyuki ; Mizuhata, Minoru

Improved cycling performance of intermetallic anode by minimized SEI layer formation

Hiroko Kuwata[1], Masaki Matsui[1,2], Hidetoshi Sonoki[1], Yusuke Manabe[1], Nobuyuki Imanishi[1] and Minoru Mizuhata[2]

1. Department of Chemistry, Mie University
   1577 Kurimamachiya-cho, Tsu, 514-8507, Mie, JAPAN
2. Department of Chemical Science and Engineering, Kobe University
   1-1 Rokkodai-cho, Nada-ku, Kobe, 657-8501, Hyogo, JAPAN

Corresponding Author: Masaki Matsui
Affiliation: Department of Chemical Science and Engineering, KOBE University
phone & fax: +81-78-803-6160
e-mail: matsui@godzilla.kobe-u.ac.jp

Abstract

Electrochemical properties of bismuth composite electrode are investigated as potential negative electrode for lithium ion batteries. The electrode shows severe capacity decay typically observed in the case of alloy-based materials, using a conventional carbonate-based electrolyte solution. The electrode maintained only 10 % of the theoretical capacity after 25 cycles of lithiation/delithiation process. The electrode shows poor coulombic efficiency of < 90% during the initial 15 cycles. On the other hand, the bismuth composite electrode shows excellent cycling performance in the 2M $LiBH_4$ in THF solution. The electrode maintained >98% of reversible capacity, even after 50 cycles. The bismuth electrode cycled in the $LiBH_4$ electrolyte maintained relatively large bismuth particles compared with the electrode cycled in the carbonate-based electrolyte. *In situ* FTIR study proved the carbonate-based electrolyte forms passivation layer <0.7 V vs. Li, while the $LiBH_4$ electrolyte does not passivate the electrode surface.

Key Words

Intermetallic anodes

Solid electrolyte interphase

Cycling performance

In situ FTIR spectroscopy

1. Introduction

Lithium-ion batteries for automotive applications have been expanding due to the commercialization of plug in hybrid vehicles and pure electrical vehicles during the last decade. Due to the increasing demands of the energy density for the long mile range electrical vehicle, alloy anodes including intermetallic anode, such as Si, Sn, Sb or Al, have been widely studied to replace the standard graphite anode, because these anode active materials theoretically have much higher specific capacity than the graphite anodes. The biggest challenge of the alloy/intermetallic anode is its cycleability. Huge volume expansion/shrinkage during the lithiation/delithiation process leads the pulverization of the active material particles resulting in loss of the electric contact among active materials, conductive carbon and current collector in the composite electrode.

In order to improve the cycling performance of the alloy anode with high specific capacity, several approaches for the electrode design were tried. The simple and the most practical approach is utilization of new binder material such as carboxyl methyl cellulose (CMC) -styrene butadiene rubber (SBR) [1], alginate [2 3], poly acrylic acid (PAA)[4], polyimide [5] and so forth. Since these binder materials show highly adhesive properties compared with polyvinylidene fluoride (PVdF), the active material particles are able to maintain electrical contact with conductive carbon and current collector even after pulverization of the particles. Another approach is micro- and nanostructural control using 1D or 2D nanomaterials [6, 7], which show isotropic volume expansion to release the internal stress.

The electrode/electrolyte interphase is important aspect for the cycleability of the alloy anode, as well. Since redox potential of the anodes are typically <1.0 V vs. Li, solid electrolyte interphase (SEI) layer is formed. In addition, the surface area of the anode continuously changes accompanied with the volume expansion/shrinkage during the charge/discharge process, hence the SEI layer needs to be physically flexible. Several research group reported the spectroscopic study of the SEI layer on the Si anode using fluoroethylene carbonate (FEC) or vinylene carbonate (VC) as electrolyte additives [8-13]. Even with these reports concerning the characterization of the SEI layer, the required physical properties of the SEI layer is still not understood yet.

In order to understand the influence of the SEI layer to the cycleability of the alloy anodes, we think the analogy of Mg-based system is useful, because the organohaloaluminate electrolyte solution, which is commonly used in the Mg-based system, does not form the

typical SEI layer [14]. In addition, Arthur *et al.* reported that Mg_3Bi_2 intermetallic anode, in the organohaloaluminate electrolyte solution, shows excellent cycleability even at the charge/discharge rate of 1C [15]. Hence, an electrolyte solution, which does not form the SEI layer is expected to improve the cycling performance of the alloy/intermetallic anodes in the Li system, as well.

Here we investigated unique electrochemical properties of lithium borohydride ($LiBH_4$) dissolved in tetrahydrofuran (THF) as a model electrolyte solution, which is unlikely to form the typical SEI layer due to its excellent reduction stability. Even though the narrow electrochemical window hinders the $LiBH_4$ electrolyte to be compatible with the conventional cathode active materials such as $LiCoO_2$ or $LiFePO_4$ and makes it difficult to be used as a practical battery electrolyte, the $LiBH_4$ electrolyte could be useful to mimic the electrode/electrolyte interphase in Mg system, using $Mg(BH_4)_2$ dissolved in ether-based solvents[16]. Therefore, we expect that the cycling performance the alloy/intermetallic anodes should be improved in the $LiBH_4$ electrolyte. In the present study, a comparative study of the Bi-based intermetallic anode in the $LiBH_4$-based electrolyte and the conventional carbonate-based solution, was carried out to discuss the role of the SEI layer against the alloy/intermetallic anodes. In addition, a spectroscopic study using *in situ* FTIR was carried out to compare the SEI formation process in the conventional carbonate electrolyte solution to the $LiBH_4$-based electrolyte solution.

2. Materials and methods

2.1. Preparation of Bi composite electrode

The electrode slurry was prepared by mixing 85 wt.% of Bi powder (99.999 %, Alfa Aesar) and 10 wt.% of acetylene black (Super P® Li, TIMCAL Graphite & Carbon), 3.5 wt.% of carboxylmethyl cellulose (CMC Daicel 2200, Daicel FineChem) and 1.5 wt.% of styrene butadiene rubber (TRD2001, JSR) with adequate amount of distilled water. The Bi powders are put through a sieve with 0.032 mm of nominal sieve opening, to remove large particles. The slurry was coated on a copper foil, and dried at 80ºC in air for 2 hours. Subsequently the electrodes punched and pressed vacuum dried at 150ºC for overnight. The loading level of the active material is 5.5-6.0 mg cm^{-2}.

2.2. Electrochemical measurements of Bi powder electrode

The electrochemical tests were conducted using a two-electrode cell (TJ-AC,

Tomcell Japan). The conventional carbonate electrolyte solution: 1 mol dm^{-3} $LiPF_6$ EC:DEC 1:1 vol.% (Kishida Chemical) and the $LiBH_4$-based solution: 2 mol L^{-1} $LiBH_4$ in THF (Sigma Aldrich) solution are employed for the lithium-based electrolyte solution. Galvanostatic charge/discharge tests were performed using a standard charger (TOSCAT-3100, Toyo system). The charge/discharge current for the initial three cycles is C/20 (=19.25 mA g^{-1}/Bi) based upon the theoretical capacity of bismuth and the voltage range was set between 0.5 and 1.2 V at room temperature. Subsequently cycling tests were performed at 1C (=385 mA g^{-1}/Bi) for 50 cycles.

2.3. in situ FTIR spectroscopy

In situ FTIR spectroscopy was carried out to detect the formation process of the SEI layer. The *in situ* FTIR measurements were carried out using a standard laboratory FTIR spectrometer (Nicolet™ iS™50 FTIR, ThermoFisher Scientific) with an MCT-detector. An spectroelectrochemical cell based on diamond ATR (DuraSamplIR II, Smiths Detection) set up was employed for the *in situ* FTIR measurement with . Detailed *in situ* FTIR set up is reported in our previous paper[14]. As a working electrode, a Ni thin film electrode was coated on the diamond window using DC sputtering coater (E-1010, Hitachi High Technologies). The lithium foil was employed for the reference and the counter electrode.

The spectroelectrochemical measurements were carried out during CV measurements of the sweep rate at 0.2 mV sec^{-1}. The CV measurement for the conventional carbonate-based electrolyte was taken between the open circuit potential (OCP): 3.11 V vs. Li/Li^+ and 0.0 V vs. Li/Li^+. Since the $LiBH_4$ electrolyte is oxidized around 2.0 V vs. Li/Li^+, the cyclic voltammograms of the $LiBH_4$ electrolyte was taken between the OCP: 1.7 V vs. Li/Li^+ and 0.0 V vs. Li/Li^+. Each FTIR spectrum was taken by the single beam mode. Subtractive normalized interfacial FTIR (SNIFTIR) spectrum was calculated by the following equation,

$$\Delta R=(R_{n+1}-R_n)/R_n \quad (1)$$

where R_n is a reference reflective spectrum and R_{n+1} is a reflective spectrum at a target electrode potential. In the present study, R_n is corresponding to specific electrode potential, hence we label each SNIFTIR spectrum as (R_{n+1} V, R_n V). If we take a spectrum at 2.8 V after 3.1 V during a cathodic scan, the SNIFTIR spectrum is labeled as (2.8 V, 3.1 V).

3. Results and discussion

3.1. Charge/discharge curves of Bi composite electrodes

Fig. 1 shows galvanostatic charge/discharge curves of the Bi composite electrodes in the conventional carbonate-based electrolyte solution (a) and the $LiBH_4$-based electrolyte solution (b). The charge/discharge curve of the Bi composite electrode has two plateaus. The 1st plateau is corresponding to the two-phase reaction between Bi and LiBi and the 2nd plateau is corresponding to the LiBi-Li_3Bi two-phase reaction. Besides these two major plateaus, an irreversible capacity of 15-20 mAh g^{-1}, is observed at the very beginning of the initial lithiation process between 1.8 and 1.4 V vs. Li/Li^+. Since the voltage range of the reaction is same in both of the electrolyte solutions, we suspect the irreversible capacity is corresponding to the reduction of the native oxide layer at the surface of the Bi particles.

The Bi composite electrode in the carbonate-based electrolyte solution exhibits charge (lithiation) capacity of 421 mAh g^{-1} and discharge (delithiation) capacity of 341 mAh g^{-1} at the 1st cycle. Considering the initial irreversible capacity of 19 $mAhg^{-1}$ corresponding to the reduction of the native oxide layer, the extra irreversible capacity of 61 mAh g^{-1} is probably corresponding to the reduction of the electrolyte solution to form an SEI layer during the initial lithiation process. In the following cycle, the Bi composite electrode showed the charge capacity of 347 mAh g^{-1} and the discharge capacity of 352 mAh g^{-1}, respectively. The excess delithiation capacity is probably due to the remained lithium after the 1st delithiation process. Improved reversibility of the Bi electrode at the 2nd cycle also indicates that the stable SEI layer is formed during the 1st cycle.

On the other hand, the Bi composite electrode in the $LiBH_4$ electrolyte shows charge capacity of 386 mAh g^{-1} and discharge capacity of 391 mAh g^{-1}, respectively. At glance the $LiBH_4$ electrolyte showed excellent reversibility compared with the conventional carbonate-based electrolyte solution, with excess coulombic efficiency of 101.3%. Considering the hidden irreversible capacity of 15 mAh g^{-1}, during the initial lithiation process, the excess irreversible discharge capacity is estimated to 20 mAh g^{-1}.

The excess discharge capacity in the $LiBH_4$ electrolyte, suggests that either slight oxidation of the electrolyte solution during the delithiation process, or self lithiation of the Bi composite electrode before the charge/discharge process, occurred. In this system, the reduction of the $LiBH_4$ electrolyte during the lithiation process is negligible. In

addition, the electrode/electrolyte interphase is mostly maintained as SEI layer free (or very thin SEI layer). The coulombic efficiency at the 2nd cycle is 101.9%, with the charge capacity of 382 mAh g^{-1} and the discharge capacity of 375 $mAhg^{-1}$. A similar irreversible reaction as the 1st cycle took place during the 2nd lithiation/delithiation process.

3.2. Cycling performance of the Bi composite electrodes

The cycling performances of the Bi composite electrodes in the two electrolyte solutions are shown in Fig. 2. The Bi composite electrode with the conventional carbonate-based electrolyte solution shows poor cycling performance as shown in Fig.2 (a). The electrode initially showed reversible capacity of 270 mAh g^{-1}, showing that the capacity decay immediately begins during the cycling test. The reversible capacity dropped to 77 mAh g^{-1} after 10th cycle, and <10 mAh g^{-1} after the 45h cycle. Fig 2 (b) shows the cycling performance of the Bi composite electrode in the $LiBH_4$-based electrolyte solution. The initial cycle showed reversible capacity of 386 mAh g^{-1} and maintained >95% of the reversible capacity even after the cycling test. In the analogy of the Mg-based system, we attribute the excellent cycleability of the $LiBH_4$-based electrolyte solution largely to the electrode/electrolyte interphase, because the cell maintained high coulombic efficiency during the cycling test, while the carbonate-based electrolyte solution continuously showed low coulombic efficiency 80-95%.

Fig. 3 shows SEM images of the as-obtained Bi powder (a) and the Bi composite electrodes after the cycling test (b), (c). The Bi particles in the composite electrodes are severely pulverized after the cycling test in both of the electrolyte solutions. The Bi electrode cycled in the carbonate-based electrolyte solution has the smallest submicron sized particles, while the $LiBH_4$ electrolyte maintains 1-5 μm size particles. We suspect the SEI layer in the carbonate-based electrolyte solution accelerates the pulverization of the Bi particles. Once the SEI layer is formed at the new surface of the pulverized particles, the interparticle connection is broken to form the electrically isolated particles, which causes the severe capacity fading of the electrode. The smaller particle size of the Bi composite electrode in the carbonate-based electrolyte solution suggests that the electrode has more isolated particles than the other two electrodes due to the formation of the SEI layer.

3.3. In situ FTIR spectroscopy for the SEI layer formation process

In order to compare the SEI formation process in the two electrolyte solutions, we conducted *in situ* FTIR spectroscopy. Fig. 4 shows *in situ* FTIR spectra of Ni thin film electrode in the conventional carbonate-based electrolyte solution. The SNIFTIR spectra for the carbonate-based electrolyte shows relatively weak peaks above 0.7 V vs. Li/Li^+ during the initial cathodic scan. All those positive and negative peaks are corresponding to the adsorbed EC and DEC molecules at the surface of the electrode. Subsequently, strong positive and negative peaks appeared <0.7 V vs. Li. The strong positive peaks at 1800, 1766 and 1735 cm^{-1} are assigned to the C=O stretching vibration in EC or DEC. The peaks at 1257 and 1155 cm^{-1} are assigned to the C-O asymmetric stretching vibration in EC or DEC. The peak at 1076 cm^{-1} is corresponding to C-O symmetric vibration in DEC, the peak at 842 cm^{-1} is corresponding to P-F stretching vibration in PF_6^- anion. The negative peaks at 1101 and 916 cm^{-1} are corresponding to the new products by decomposed EC or DEC, and the peak at 831 cm^{-1} is assigned to the decomposed PF_6^- anion. Negative peaks around 1400 cm^{-1} are corresponding to the carboxylate derivatives of the decomposed EC or DEC. A summary of the peak assignments for the conventional carbonate electrolyte is shown in Table 1 [17]. Since the SNIFTIR spectra for the subsequent anodic scan show only small peaks at 779, 842, and 1072 cm^{-1}, suggesting that the electrode surface is mostly passivated by the surface layer formed at <0.7 V vs. Li/Li^+ during the initial cathodic scan. In the following cycle, the SNIFTIR spectra showed several positive and negative peaks. The peak intensity of the SNIFTIR spectra >0.7 V vs. Li/Li^+ is relatively higher than the 1st cycle, while very strong peaks at low electrode potential <0.3 V vs. Li/Li^+ did not appear, because the surface of the Ni electrode is already passivated with the SEI layer. All the positive peaks observed in the 2nd cycle, are assigned to either EC, DEC or PF_6^- anion in the electrolyte solution. Two broad negative peaks around 1400-1600 cm^{-1} are observed only at low electrode potential <0.3 V vs. Li/Li^+. The peaks are probably corresponding to the decomposed products of the electrolyte solution at low electrode potential. The continuous decomposition of the electrolyte solution during the multiple cycles is in good agreement with the continuous low coulombic efficiency of the Bi composite electrode in the carbonate-based electrolyte solution through long cycling.

Fig. 5 shows the SNIFTIR spectra of the $LiBH_4$-based electrolyte solution during

CV measurement. During the initial cathodic scan, a positive peak at 1400 cm^{-1} and a negative peak at 1260 cm^{-1} are continuously observed. Both of the two peaks are assigned to the lattice vibration of the crystalline $LiBH_4$ [18]. A small positive peak at 1060 cm^{-1} is assigned to C-O-C asymmetric stretching vibration of THF molecule. A summary of the peak assignment for the $LiBH_4$-based electrolyte solution is shown in Table. 2. Furthermore, these two peaks subsequently flipped during the anodic scan >1.4 V vs. Li. Since the reversible spectrum change is also observed in the 2nd cycle as shown in Fig. 5 (b), we assume that the adsorbed BH_4^- anion at the surface of the electrode, forms an ordered phase, which shows reversible phase transition upon the electrode potential. Further structural analyses are necessary to understand the dynamic behavior of the electrode/electrolyte interphase. Other peaks in the SNIFTIR spectra also showed the dynamic behavior of the THF molecules. The positive peak at 1060 cm^{-1} is assigned to C-O-C asymmetric stretching vibration of the THF molecules during the cathodic scan. The small negative peak approx. 20 cm^{-1} below the positive peak is corresponding to the adsorption of the THF molecules at the surface of the electrode. Both of these peaks also flip during the anodic scan and following cycle. Such reversible spectra changes during the cyclic voltammetry are obviously very different from the spectra observed in the carbonate-based electrolyte solution. Furthermore, the dynamic behavior of the electrode/electrolyte interphase, is typically observed in the electrolyte solution, which does not form the typical SEI layer like Mg-based system. Therefore, we conclude that the $LiBH_4$-based electrolyte solution is a kind of the minimized SEI formation system and the excellent cycling performance of the Bi composite electrode in the $LiBH_4$-based electrolyte solution is mainly due to the very thin SEI layer.

4. Conclusion

In the present study, we investigated how the SEI layer affects to the cycling performance of the intermetallic anode using the Bi composite electrode in the conventional carbonate-based electrolyte solution and the $LiBH_4$-based electrolyte solution. The electrode in the conventional carbonate-based electrolyte solution shows poor reversibility and severe capacity fading, suggesting the continuous electrolyte decomposition due to the volume change of the Bi particles. On the other hand, the electrode in the $LiBH_4$-based electrolyte solution shows the excellent cycling

performance, with the high coulombic efficiency.

After the cycling test, the Bi particles in the composite electrodes are severely pulverized. The electrode cycled in the carbonate-based electrolyte solution especially has the smaller particle size compared with other electrodes. We suspect the SEI layer formed at the surface of the pulverized particles initiates the electrical isolation of the particles in the electrode, resulting in the capacity fading.

In situ FTIR spectroscopy was carried out to confirm the SEI formation process in the carbonate-based electrolyte solution and the $LiBH_4$-based electrolyte solution. The carbonate-based electrolyte solution showed very strong peaks corresponding to the formation of the SEI layer at the electrode potential <0.7 V vs. Li/Li^+. The *in situ* FTIR spectroscopy also proved that the $LiBH_4$-based electrolyte solution does not form typical SEI layer.

Acknowledgement

The present study was financially supported by Japan Science and Technology Agency PRESTO (Grant No. JPMJPR13CA) and CREST feasibility study for Revolutional Materials Development.

Figure Captions

Fig. 1 Galvanostatic charge/discharge curves of Bi-Li half-cells using 1 M $LiPF_6$ in EC:DEC (1:1 vol.%) (a) and 2 M $LiBH_4$ in THF (b). The charge/discharge current is 19.25 mAg-1 (= C/20 of the theoretical capacity of the bismuth)

Fig. 2 Cycling performance of the Bi-Li half-cell with 1 M $LiPF_6$ in EC:DEC (1:1 vol.%) (a) and 2 M $LiBH_4$ in THF (b). The charge/discharge current is 385 mAg^{-1} (1C of the theoretical capacity of the bismuth)

Fig. 3 SEM images of the as-obtained Bi powders (a), the electrode cycled in the conventional carbonate-based electrolyte solution (b) and the $LiBH_4$-based electrolyte solution (c), for 50 cycles

Fig. 4 *In situ* FTIR spectra of Ni thin film electrode in the conventional carbonate-based electrolyte solution. The CV measurement was taken between the initial open circuit

potential (OCP) and 0 V vs. Li/Li^+. The OCP is 3.11 Vvs.Li/Li^+ for two cycles.

Fig. 5 *In situ* FTIR spectra of Ni thin film electrode in the $LiBH_4$-based electrolyte solution. The CV measurement was taken between the initial open circuit potential (OCP) and 0 V vs. Li/Li^+. The OCP is 1.85 V vs. Li/Li^+ for two cycles.

Reference

1. J. Li, R. B. Lewis and J. R. Dahn, *Electrochemical and Solid-State Letters*, **10** (2007).
2. I. Kovalenko, B. Zdyrko, A. Magasinski, B. Hertzberg, Z. Milicev, R. Burtovyy, I. Luzinov and G. Yushin, *Science*, **334**, 75 (2011).
3. M. H. Ryou, J. Kim, I. Lee, S. Kim, Y. K. Jeong, S. Hong, J. H. Ryu, T. S. Kim, J. K. Park, H. Lee and J. W. Choi, *Adv Mater*, **25**, 1571 (2013).
4. Z. J. Han, K. Yamagiwa, N. Yabuuchi, J. Y. Son, Y. T. Cui, H. Oji, A. Kogure, T. Harada, S. Ishikawa, Y. Aoki and S. Komaba, *Phys Chem Chem Phys*, **17**, 3783 (2015).
5. H. S. Yang, S. H. Kim, A. G. Kannan, S. K. Kim, C. Park and D. W. Kim, *Langmuir*, **32**, 3300 (2016).
6. C. K. Chan, H. Peng, G. Liu, K. McIlwrath, X. F. Zhang, R. A. Huggins and Y. Cui, *Nature Nanotechnology*, **3**, 31 (2008).
7. M. Saito, T. Yamada, C. Yodoya, A. Kamei, M. Hirota, T. Takenaka, A. Tasaka and M. Inaba, *Solid State Ionics*, **225**, 506 (2012).
8. N.-S. Choi, K. H. Yew, K. Y. Lee, M. Sung, H. Kim and S.-S. Kim, *Journal of Power Sources*, **161**, 1254 (2006).
9. L. Chen, K. Wang, X. Xie and J. Xie, *Journal of Power Sources*, **174**, 538 (2007).
10. C. K. Chan, R. Ruffo, S. S. Hong and Y. Cui, *Journal of Power Sources*, **189**, 1132 (2009).
11. B. Philippe, R. Dedryvère, J. Allouche, F. Lindgren, M. Gorgoi, H. Rensmo, D. Gonbeau and K. Edström, *Chemistry of Materials*, **24**, 1107 (2012).
12. B. Philippe, R. Dedryvere, M. Gorgoi, H. Rensmo, D. Gonbeau and K. Edstrom, *J Am Chem Soc*, **135**, 9829 (2013).
13. M. Nie, D. P. Abraham, Y. Chen, A. Bose and B. L. Lucht, *The Journal of Physical Chemistry C*, **117**, 13403 (2013).
14. H. Kuwata, M. Matsui and N. Imanishi, *Journal of The Electrochemical Society*, **164**, A3229 (2017).

15. T. S. Arthur, N. Singh and M. Matsui, *Electrochemistry Communications*, **16**, 103 (2012).
16. R. Mohtadi, M. Matsui, T. S. Arthur and S.-J. Hwang, *Angewandte Chemie-International Edition*, **51**, 9780 (2012).
17. M. Matsui, S. Deguchi, H. Kuwata and N. Imanishi, *Electrochemistry*, **83**, 874 (2015).
18. K. B. Harvey and N. R. Mcquaker, *Canadian Journal of Chemistry*, **49**, 3282 (1971).

Table 1 Summary of the peak assignments of the *in situ* FTIR spectra for 1 M $LiPF_6$ EC:DEC (1:1 vol.%) solution during cathodic scan

cm^{-1}	
	Positive Peaks
1800	C=O stretching vibration in EC
1766	C=O stretching vibration in EC
1735	C=O stretching vibration in DEC
1556	C-H bending vibration in EC
1471	C-H bending vibration in EC
1409	C-H bending vibration in adsorbed or solvated EC or DEC
1384	C-H bending vibration in EC
1380	C-H bending vibration in DEC
1295	C-O asymmetric stretching vibration in adsorbed or solvated DEC
1257	C-O asymmetric stretching vibration in DEC
1189	C-O asymmetric stretching vibration in adsorbed or solvated EC
1155	C-O asymmetric stretching vibration in EC
1076	C-O symmetric stretching vibration in DEC
1020	C-O symmetric stretching vibration in DEC
975	C-O symmetric stretching vibration in EC
906	C-H bending vibration in DEC
842	P-F stretching vibration in $LiPF_6$
798	C-H bending vibration in DEC
779	C-H bending vibration in EC
725	C-H bending vibration in adsorbed or solvated EC
719	C-H bending vibration in EC
	Negative peaks
1563-1344	Carboxylate derivatives of the decomposed EC or DEC
1101	C-O symmetric stretching vibration in decomposed DEC
916	C-H bending vibration in decomposed DEC
831	P-F stretching vibration in decomposed $LiPF_{6spectroscopic}$

Table 2 Summary of the peak assignments of the *in situ* FTIR spectra for the 2 M $LiBH_4$ THF solution during cathodic scan

cm^{-1}	
	Positive Peaks
1400	Lattice vibration of the $LiBH_4$
1060	C-O-C asymmetric stretching vibration of THF
835	C-H bending vibration of THF
730	$LiBH_4$-THF complex
	Negative peaks
1260	Lattice vibration of the $LiBH_4$
1025	C-O-C asymmetric stretching vibration of adsorbed THF
885	C-H bending vibration of THF
761	adsorbed $LiBH_4$-THF complex

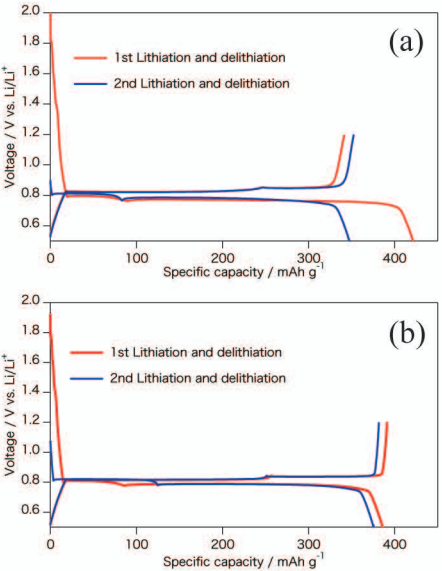

Fig. 1 Galvanostatic charge/discharge curves of a Bi-Li half-cells using 1 M $LiPF_6$ in EC:DEC (1:1 vol.%) (a) and 2 M $LiBH_4$ in THF (b). The charge/discharge current is 19.25 mAg^{-1} (= C/20 of the theoretical capacity of the bismuth)

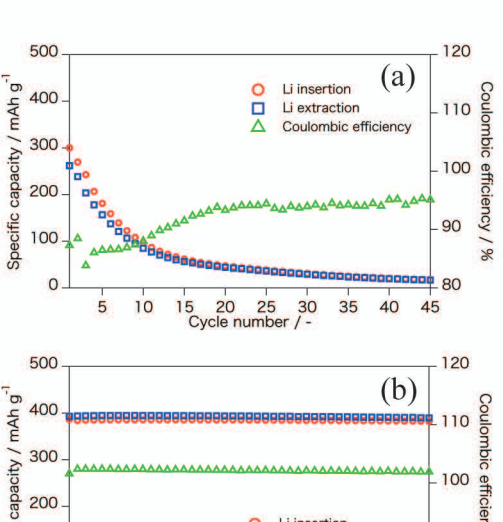

Fig. 2 Cycling performance of the Bi-Li half-cell with 1 M $LiPF_6$ in EC:DEC (1:1 vol.%) (a) and 2 M $LiBH_4$ in THF (b). All the half-cells were operated at the current 385 mA g^{-1} (1C per bismuth)

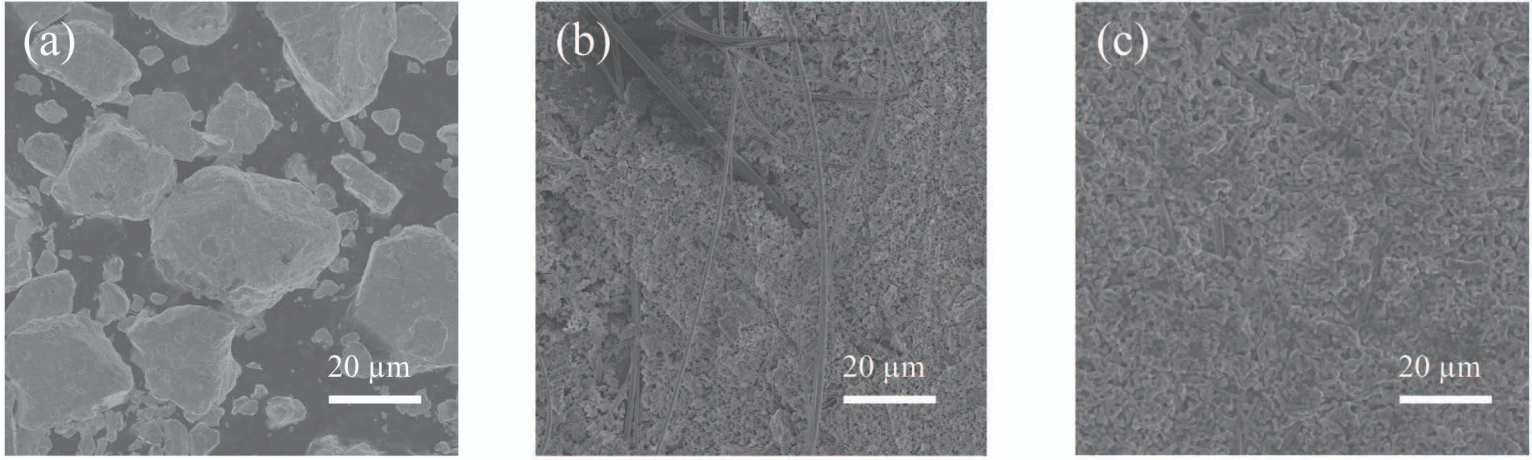

Fig. 3 SEM images of as received bismuth powder (a), the composite electdoe

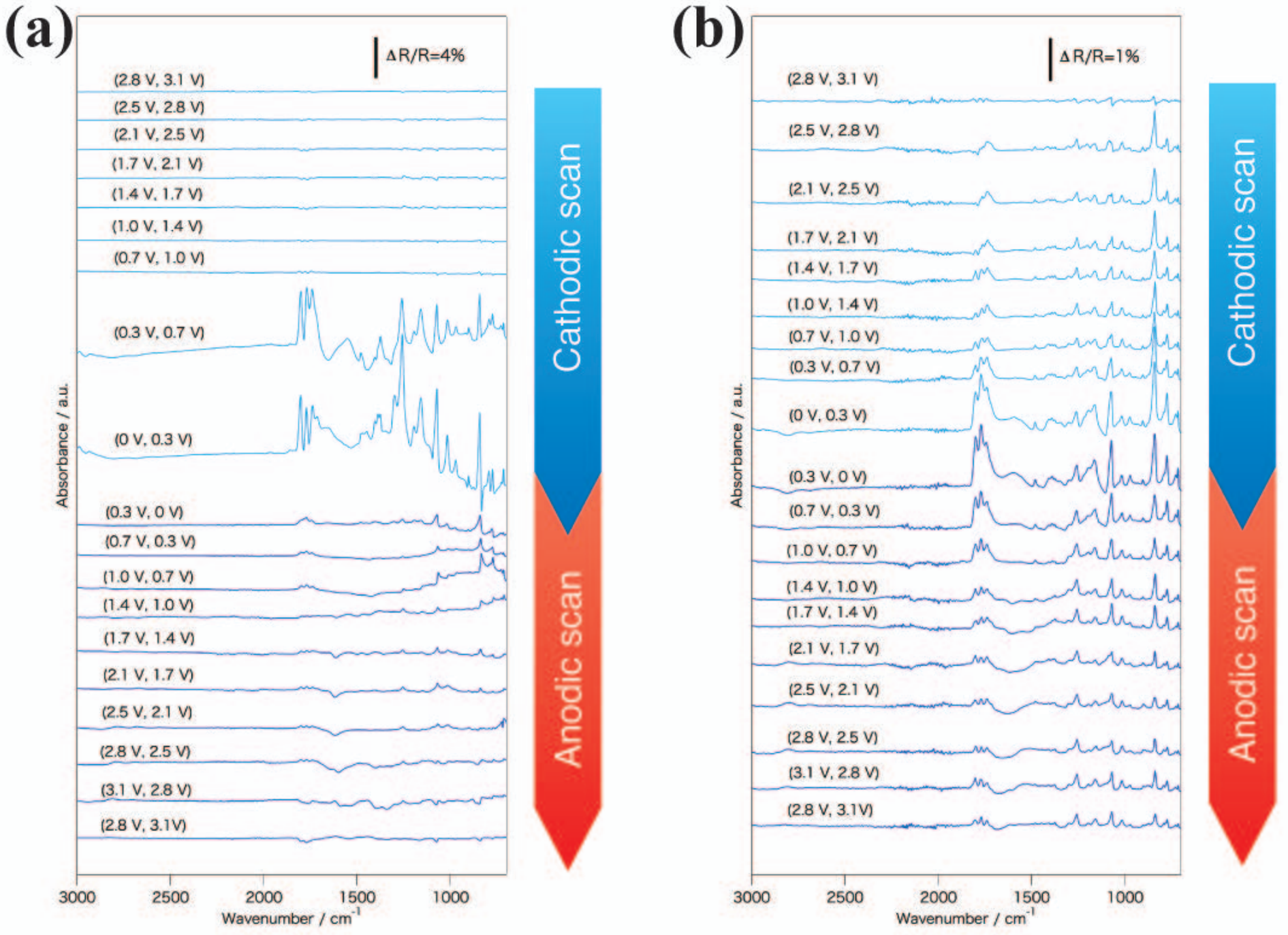

Fig. 4 *In situ* FTIR spectra of Ni thin film electrode in the conventional carbonate-based electrolyte solution. The CV measurement was taken between the initial open circuit potential (OCP) and 0 V vs. Li/Li^+. The OCP is 3.11 Vvs.Li/Li^+ for two cycles.

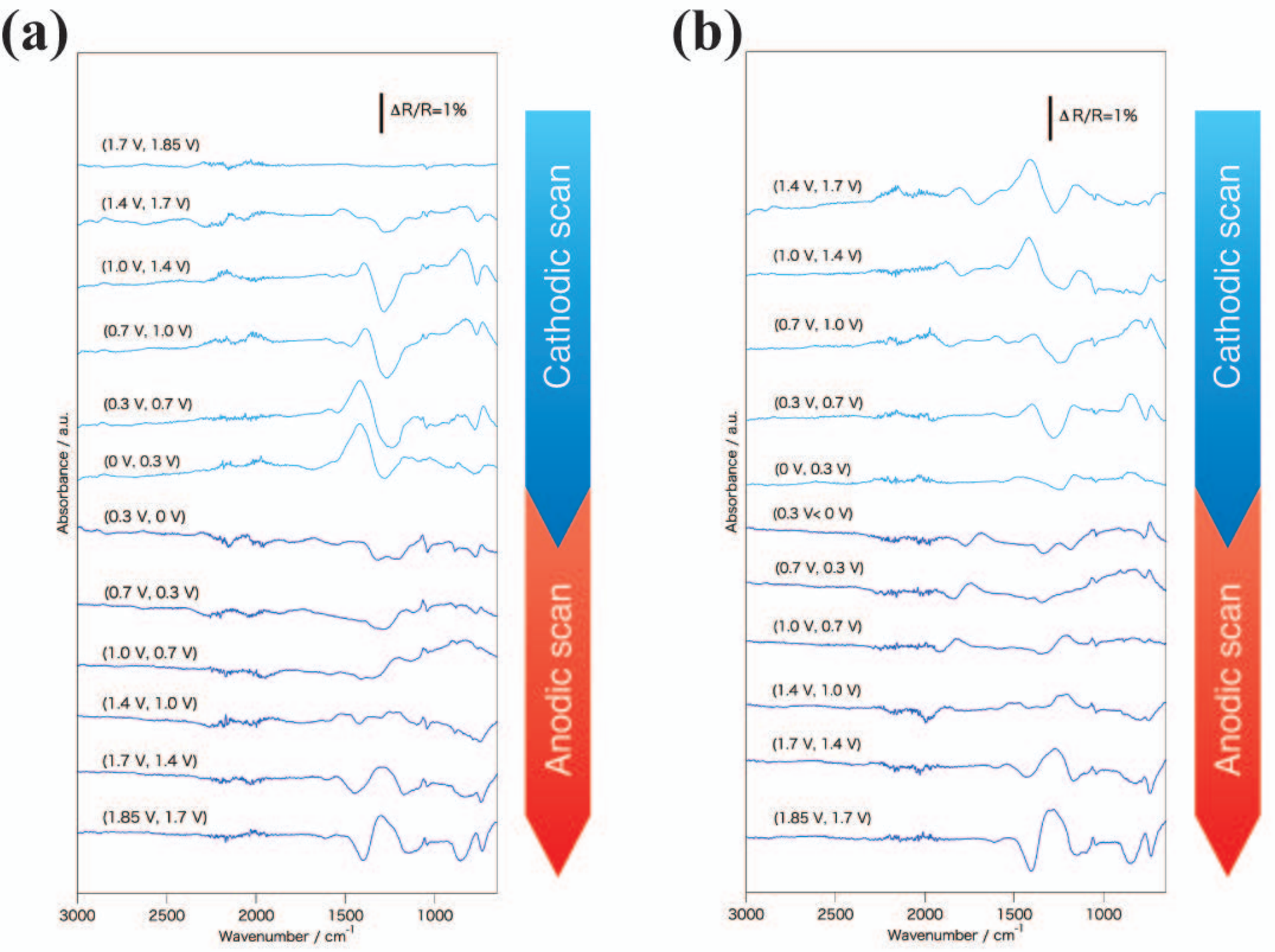

Fig. 5 *In situ* FTIR spectra of Ni thin film electrode in the $LiBH_4$-based electrolyte solution. The CV measurement was taken between the initial open circuit potential (OCP) and 0 V vs. Li/Li^+. The OCP is 1.85 V vs. Li/Li^+ for two cycles.